



## OPEN ACCESS

## EDITED BY

Manuel Alcázar-Ortega,  
Universitat Politècnica de València, Spain

## REVIEWED BY

Linfei Yin,  
Guangxi University, China  
Lina Montuori,  
Universitat Politècnica de València, Spain

## \*CORRESPONDENCE

Tengfei Wei,  
✉ tfwei@lut.edu.cn

RECEIVED 13 November 2023

ACCEPTED 05 January 2024

PUBLISHED 05 February 2024

## CITATION

Wei T, Wang Y and Yang J (2024), Distributed ADMM power optimal control for standalone hybrid generation systems. *Front. Energy Effic.* 2:1337606. doi: 10.3389/fenef.2024.1337606

## COPYRIGHT

© 2024 Wei, Wang and Yang. This is an open-access article distributed under the terms of the [Creative Commons Attribution License \(CC BY\)](https://creativecommons.org/licenses/by/4.0/). The use, distribution or reproduction in other forums is permitted, provided the original author(s) and the copyright owner(s) are credited and that the original publication in this journal is cited, in accordance with accepted academic practice. No use, distribution or reproduction is permitted which does not comply with these terms.

# Distributed ADMM power optimal control for standalone hybrid generation systems

Tengfei Wei\*, Yiyang Wang and Jichang Yang

School of Electrical and Information Engineering, Lanzhou University of Technology, Lanzhou, China

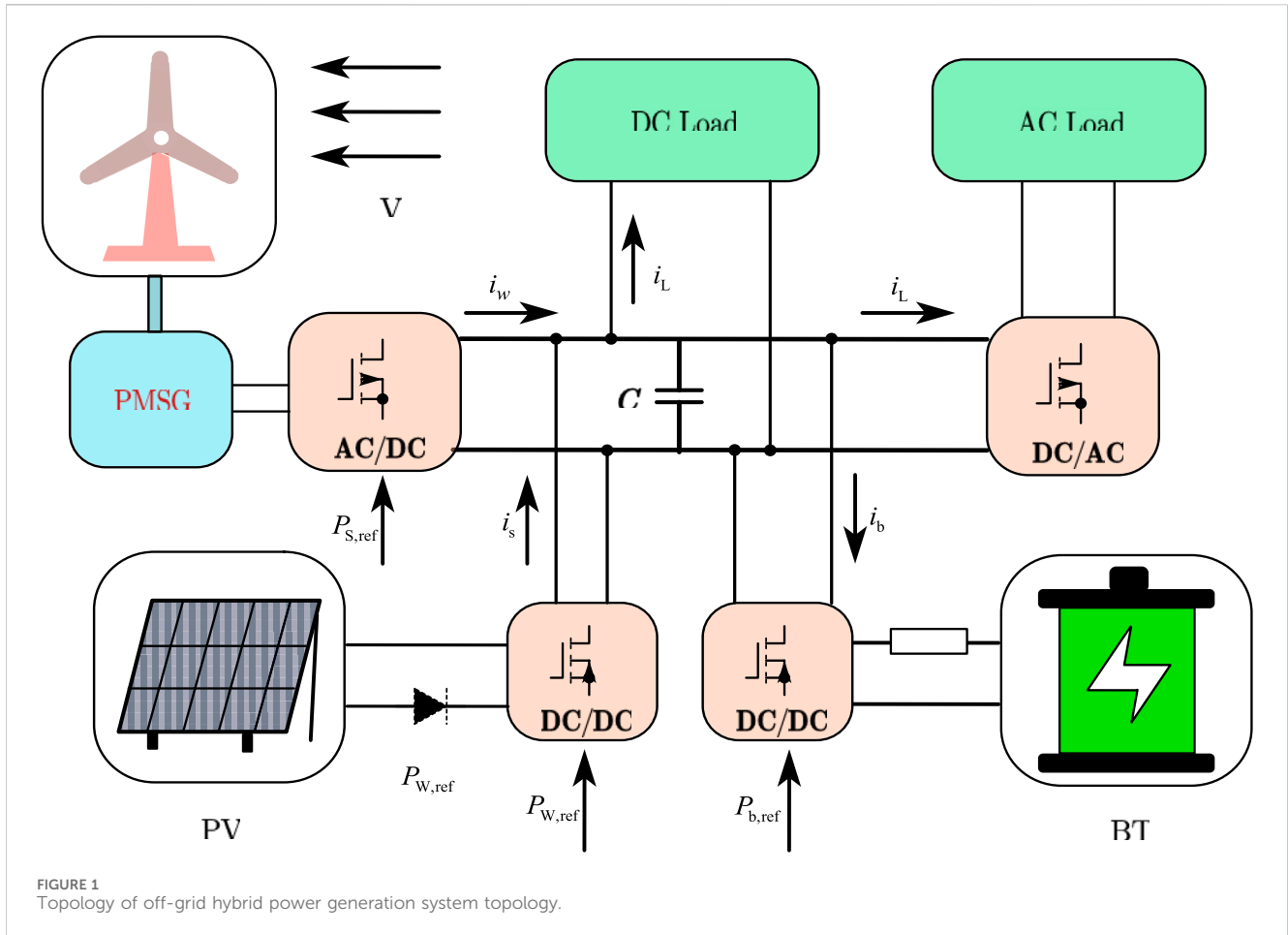
With the rapid development and increased demand for renewable energy sources, standalone hybrid generation systems have become an essential energy solution. Power optimization control is thus critical to achieving the efficient operation and stability of this system. The distributed ADMM (alternating direction method of multipliers)-based approach has the full potential to deal with the power optimization problem of standalone hybrid generation systems. This study uses an optimization algorithm with a Gaussian penalty function, ADMM- $\rho$ , to alternately optimize the power reference values of wind, light, and battery-containing power generation subsystems. The local controller regulates the output power of the converter according to this reference value. This ensures that the wind and photovoltaic power generation subsystem work in load-tracking or maximum power-tracking modes so that the optimal operation of hybrid power generation meets the balance of supply and demand while prolonging the service life of the batteries. Simulation experiments show that the distributed ADMM algorithm can reliably address the power optimization challenge of hybrid power generation systems.

## KEYWORDS

standalone hybrid generation systems, distributed ADMM, power optimal control, renewable energy source, optimal power allocation

## 1 Introduction

Due to current problems of environmental pollution and energy scarcity, wind and solar energy, rich in reserves, have attracted more attention as crucial clean energy sources to effectively cope with the energy crisis and environmental problems (Suo et al., 2021). In order to meet the balance between power generation and the load power of off-grid hybrid systems, maximizing the use of clean energy resources while considering and extending battery service life can make a whole system operate more efficiently and reduce operating costs; the key is the optimal power distribution of each power generation unit. Therefore, much research has studied the optimal power allocation of standalone hybrid generation systems. Feroldi and Zumoffen (2014) optimized the control of the operating mode of each generating unit of a standalone hybrid wind, solar, and storage power generation system to ensure power balance between the generating units and the loads. Feroldi et al. (2015) proposed an optimal management strategy for batteries in power generation systems that can consider a battery's state of charge between reasonable upper and lower limits to ensure that it does not overshoot and over-discharge to prolong its service life and ensure its safe operation. Zhao and Yuan (2016) proposed a fruit fly optimization algorithm based on power optimization allocation control to achieve multi-objective optimization with the simultaneous minimization of annual power generation costs and CO<sub>2</sub> emissions. Wang



et al. (2017a) used a hierarchical control structure with distributed predictive control to achieve optimal power allocation in standalone hybrid generation systems to reduce the time cost associated with centralized optimal control and satisfy the system's power balance. Le et al. (2020) reviewed the current status and development of research on distributed model predictive controls applied in hybrid power system. Considering the power balance, output power of each power generation unit, battery state of charge, and other factors in the objective function, distributed model predictive control can optimize the output power of the coordinated multiple power generation units to achieve optimal functioning to maximize a whole hybrid power generation system's use of wind and clean energy while prolonging battery life to further improve the operating efficiency of the system and reduce operating costs.

For standalone hybrid generation systems that contain multiple types of generation units, centralized model predictive control can be used to study power optimal control problems. However, this method involves significant computation and high communication and time costs to find an optimal solution while exposing the information on each generation unit. The current approach is inadequate for protecting the privacy of a generation unit's information. To address this issue, ADMM utilizes its decomposability and fast convergence to break down large-scale and complex optimization problems into smaller sub-optimization problems. Each sub-optimization task is processed in parallel on a corresponding computing node, utilizing coordination and

cooperation among the sub-optimization tasks to enhance the efficiency of the optimization computation. However, it is important to note that ADMM may be influenced by the specific characteristics of problems and parameter selection. To address this limitation, this paper introduces a Gaussian penalty function that enhances the power optimization performance of the system by improving convergence speed.

Currently, the standard distributed optimization methods are the gradient descent method (Bottou et al., 2018), the proximal gradient descent method (Parikh, 2014), the coordinate descent method (Wright, 2015), and the alternating direction method of multipliers (ADMM). Among these, ADMM combines the advantages of decomposability and fast convergence of the multiplier method. In hybrid power generation systems, ADMM can decompose the power optimization problem of each power generation unit and, under its constraints, first solve it locally, then update the parameters in the rest of the power generation units, and finally make the hybrid power generation system work in the optimal state through the above iterations; the multiplier method in ADMM can better solve the contradiction between the good convergence of small step lengths and the non-convergence of considerable step lengths (Y. Wang et al., 2017b). It thus ensures the fast convergence of a power generation system (Chang et al., 2019). Increasing the penalty function can increase the maximum iteration step length compared with the gradient descent method, which can accelerate convergence speed (Chang et al., 2019).

ADMM is thus suitable for wind–solar–storage hybrid power generation systems, which present a power optimal control problem containing multiple generation types; by improving the ADMM algorithm to increase convergence speed, it can improve the performance of power optimal control of a hybrid power generation system (Kang et al., 2018).

We here establish mathematical models for the subsystems of wind power generation, photovoltaic generation, and batteries. We apply the ADMM algorithm to establish the objective function and constraints. The convergence speed of the ADMM algorithm is enhanced by introducing the Gaussian penalty function  $\rho$ . The resulting ADMM- $\rho$  algorithm is used to determine power reference values for wind power generation, photovoltaic power generation, and battery subsystems. The power reference values are alternately optimized, and by modifying the converter’s output power, the wind and PV power generation systems operate in load tracking or maximum power tracking mode. This results in the hybrid power generation system’s optimal operation, ensuring the balance between supply and demand while prolonging the battery’s service life.

This paper is organized as follows. Section 2 offers a mathematical model for standalone hybrid generation systems. Section 3 discusses the ADMM power optimal control framework for these systems, including the power optimization process, objective function, constraints of the ADMM optimization, and iterative design of the distributed ADMM- $\rho$ . Section 4 presents a simulation experiment utilizing WP data from a southern region of China, with load power serving as the input to simulate the proposed model. The results of the simulation experiment are then analyzed.

## 2 Mathematical modeling of standalone hybrid generation systems

Standalone hybrid generation systems consist of three subsystems: wind power generation, photovoltaic power generation, and battery (Figure 1).

The photovoltaic power generation subsystem is composed of wind turbines, permanent magnet synchronous generators (PMSGs), rectifiers, and DC/DC converters. Battery subsystems are the energy storage devices of hybrid power generation systems which are composed of batteries and DC/DC converters. The three subsystems operate in parallel via the DC buses to supply power to the DC loads, or through the inverter to supply power to the AC loads.

### 2.1 Wind electronic system model

Wind power is generated by a wind turbine that absorbs wind energy and converts it into mechanical energy in the drive chain. A generator then converts the mechanical energy into electrical energy to supply the load. According to the principle of aerodynamics, the expression of the output power of a wind turbine is expressed as follows:

$$P_t = \frac{1}{2} \rho A v_w^3 C_p(\lambda, \beta), \tag{1}$$

where  $\rho$  is the air density,  $A$  is the sweeping area of the wind turbine,  $v_w$  is the effective wind speed,  $\lambda$  is the blade tip speed ratio of the wind turbine,  $\beta$  is the pitch angle, and  $C_p(\lambda, \beta)$  is wind energy utilization, the size of which are determined by  $\lambda$  and  $\beta$  together as follows:

$$\begin{cases} C_p(\lambda, \beta) = 0.5176 \left( \frac{116}{\lambda_i} - 0.4\beta - 5 \right) e^{-\frac{21}{\lambda_i}} + 0.0068\lambda \\ \frac{1}{\lambda_i} = \frac{1}{\lambda + 0.08\beta} - \frac{0.035}{\beta^3 + 1} \\ \lambda = \frac{R\omega_0}{v} = \frac{2\pi R n_0}{v}, \end{cases} \tag{2}$$

where  $R$  is the paddle radius,  $\omega_0$  is the angular velocity of the wind turbine, and  $n_0$  is the rotational speed of the wind turbine. In this study, a fixed pitch angle wind turbine is selected, so  $\beta = 0$ .

The mathematical model of a permanent magnet synchronous generator in the DC coordinate system is established as follows:

$$\begin{cases} \dot{i}_q = -\frac{R_s}{L} i_q - \omega_e i_d + \omega_e \frac{\Phi_s}{L} - \frac{\pi v_b i_q}{3\sqrt{3} L \sqrt{i_q^2 + i_d^2}} u_w, \\ \dot{i}_d = -\frac{R_s}{L} i_d - \omega_e i_q - \frac{\pi v_b i_d}{3\sqrt{3} L \sqrt{i_q^2 + i_d^2}} u_w, \end{cases} \tag{3}$$

$$\begin{cases} \dot{\omega}_e = \frac{P}{2J} \left( T_t - \frac{3}{2} \frac{P}{2} \Phi_s i_q \right), \\ i_w = \frac{\pi v_b}{2\sqrt{3}} \sqrt{i_d^2 + i_q^2} u_w, \end{cases} \tag{4}$$

where  $i_q$   $i_d$  is the rotor-side straight-axis and cross-axis currents,  $\omega_e$  is the electromagnetic rotational speed,  $R_s$  and  $L$  are, respectively, the resistance and inductance of each phase of the stator windings,  $P$  is the number of pole pairs of the permanent magnet synchronous generator,  $J$  is the rotational inertia of the rotating part,  $\Phi_s$  is the magnetic flux of the stator windings,  $T_t$  is the wind turbine torque,  $v_b$  is the DC bus voltage,  $i_w$  is the current injected into the DC bus, and  $u_w$  is the control signal (duty cycle of the DC/DC converter).

Eq. 3 is rewritten as follows:

$$\dot{x}_w = f_w(x_w) + g_w(x_w) u_w, \tag{5}$$

where  $x_w = [i_q \ i_d \ \omega_e]^T$  is the state vector of the wind subsystem, and  $f_w = [f_{w1} \ f_{w2} \ f_{w3}]^T$ ,  $g_w = [g_{w1} \ g_{w2} \ g_{w3}]^T$  is a nonlinear vector function.

Considering that the rectifier and DC/DC converter will have a power loss of about 5% (Xin et al., 2019), the expression for the power flowing from the wind power generation subsystems to the DC bus is represented as follows:

$$P_w = 0.95 \frac{\pi v_b}{2\sqrt{3}} \sqrt{i_d^2 + i_q^2} u_w. \tag{6}$$

### 2.2 Model of the photovoltaic power generation subsystem

The model of photovoltaic power generation subsystem is as follows:

$$\begin{cases} \dot{v}_{pv} = \frac{i_{pv}}{C} - \frac{i_s}{C} u_{pv} \\ \dot{i}_s = -\frac{v_b}{L_c} + \frac{v_{pv}}{L_c} u_{pv} \\ i_{pv} = n_p I_{ph} - n_p I_{rs} \left( \exp \left( \frac{q(v_{pv} + i_{pv} R_s)}{(n_s A_c K T_2)} \right) - 1 \right), \end{cases} \quad (7)$$

where  $v_{pv}$  and  $i_{pv}$  are, respectively, the output voltage and current of the array,  $I_{ph}$  is the photogenerated current,  $R_{sh}$  is the shunt resistance of the PV cells,  $I_D$  is the current flowing through the diode,  $R_s$  is the series equivalent internal resistance of the PV cells,  $C$  and  $L_c$  are, respectively, the capacitance and inductance of the converter,  $u_{pv}$  is the control signal (duty cycle of the DC/DC converter),  $i_s$  is the current injected into the DC bus,  $K$  is the Boltzmann constant  $K = 1.38 \times 10^{-3} J/K$ ,  $n_s$  and  $n_p$  are, respectively, the number of series and shunt connections of the PV modules in the PV array,  $I_{rs}$  is the number of series and parallel connections of PV modules in the PV array,  $T_2$  is the reverse saturation current,  $q$  is the Kelvin temperature,  $m$  is the unit charge, and  $A_c$  is the P-N junction coefficient of the semiconductor device in the PV cell.

Eq. 7 can be rewritten as follows:

$$\begin{cases} \dot{x}_s = f_s(x_s) + g_s(x_s) u_{pv}, \\ h_s(x_s) = 0, \end{cases} \quad (8)$$

where  $x_s = [v_{pv} \ i_s]^T$  is the state vector of the photovoltaic power generation subsystems, and  $f_s = [f_{s1} \ f_{s2}]^T$ ,  $g_s = [g_{s1} \ g_{s2}]^T$ , and  $h_s(x_s)$  are nonlinear functions.

Considering that the power loss of the converter is around 5%, the equation for the power flowing from the photovoltaic power generation subsystems to the DC bus is represented as follows:

$$P_s = 0.95 i_s v_b. \quad (9)$$

From (7) and (9), the power of the photovoltaic power generation subsystems is controlled by  $u_{pv}$ .

### 2.3 Model of battery subsystems

Power from wind generation quickly fluctuates due to external influences; the battery subsystems, as energy storage devices (Tan et al., 2021), can quickly respond to the power changes of the wind power generation subsystems and loads. The current flowing through the battery subsystems for power generation is represented as follows:

$$i_b = \frac{\pi}{2\sqrt{3}} \sqrt{i_d^2 + i_q^2} u_w + i_s - i_L, \quad (10)$$

where  $i_L$  is the load current (A) obtained from the measurement, the battery consists of a voltage source  $e_b$  (V), series resistance  $R_b$  ( $\Omega$ ), and capacitor  $C_b$  (F), and the battery terminal voltage  $e$  is as follows:

$$v_{bt} = 0.5 \left( e_b + v_c + \sqrt{(e_b + v_c)^2 + 4v_b i_b R_b} \right), \quad (11)$$

where  $v_c$  is the voltage across capacitor  $C_b$ , and the magnitude of  $v_c$  is calculated as follows:

$$\dot{v}_c = \frac{1}{C_b} \left( \frac{\pi}{2\sqrt{3}} \sqrt{i_d^2 + i_q^2} u_w + i_s - i_L \right). \quad (12)$$

Eq. 12 can be rewritten as follows:

$$\dot{v}_c = f_c(x_w, x_s, v_c), \quad (13)$$

where  $f_c(x_w, x_s, v_c)$  is a nonlinear function.

## 3 ADMM power optimal control for standalone hybrid generation systems with wind power and storage

Under weather conditions and load variations, the subsystems of standalone hybrid generation systems calculate the output power reference values of the wind, light, and battery subsystems through the ADMM alternately and iteratively and pass the output power reference values to the local controller of these subsystems. This adopts the sliding-mode variable-structure control to change the duty cycle of the DC/DC converter and adjusts the output power of the wind, light, and battery subsystems to meet the user's load power requirements. The local controller uses a sliding mode variable structure control to change the duty cycle of the DC/DC converter to adjust the output power of the wind, light, and battery generation subsystems so that the output power of the hybrid generation systems meets the user's load power demand. We thus obtain the ADMM control structure of the standalone hybrid generation systems (Figure 2). The power reference values of the wind, PV, and battery subsystems are used as decision quantities, which are solved by the ADMM algorithm in distributed iterations. The fast convergence of the algorithm is ensured by adding Gaussian penalty variables.

### 3.1 ADMM control structure for standalone hybrid generation systems

The structural block diagram of ADMM-based hybrid power generation system control is shown in Figure 2, where the ADMM power optimization of the wind, photovoltaic, and battery subsystems constitutes the optimization layer, and the optimization layer outputs the reference power to the local controllers of these subsystems.

The objective function of the system optimization layer is first designed. Then, the ADMM optimization algorithm is applied to the wind, PV, and battery power references with alternating iterations based on historical weather prediction data (WP), including light intensity  $H_0$  ( $\frac{W}{m^2}$ ), ambient temperature  $T_1$  ( $^{\circ}C$ ), wind speed  $v$  ( $S/m^2$ ), battery state of charge (SOC), and load power. The alternating iterations ensure the rapid convergence of the optimization process.

Finally, the power reference values of the last iteration are exchanged among wind, PV, and battery, the residuals are calculated, and the residual convergence conditions are judged to obtain the optimal power reference values  $P_{w,ref}^*$ ,  $P_{s,ref}^*$ , and  $P_{b,ref}^*$  of the wind, PV, and battery subsystems.

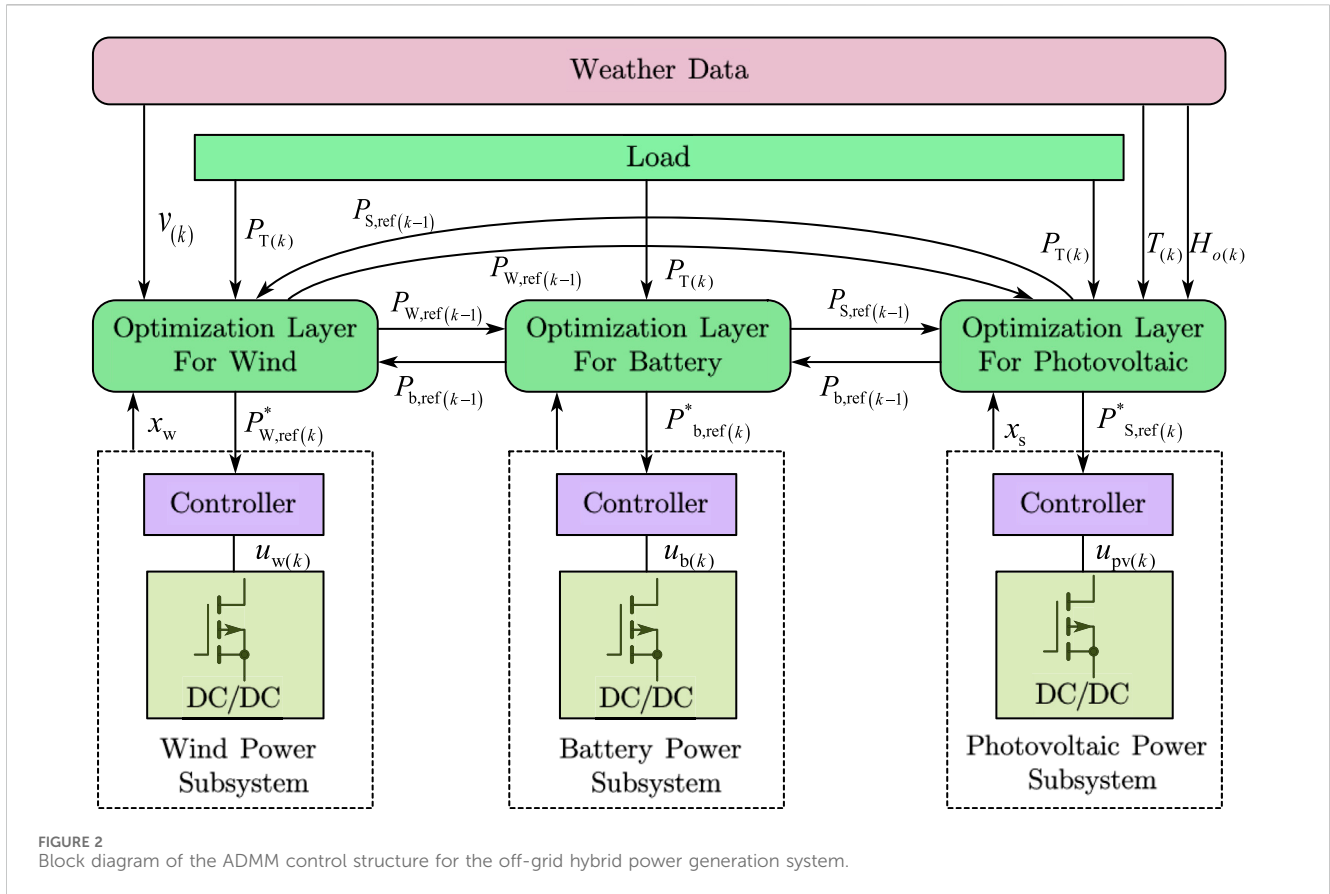


FIGURE 2 Block diagram of the ADMM control structure for the off-grid hybrid power generation system.

The optimization layer sends the optimal power reference values  $P_{W,ref}^*$ ,  $P_{S,ref}^*$ , and  $P_{b,ref}^*$  to the respective subsystem controllers, and the local controllers of the wind, photovoltaic, and battery subsystems control the duty cycles of their respective DC/DC converters according to  $P_{W,ref}^*$ ,  $P_{S,ref}^*$ , and  $P_{b,ref}^*$  using a sliding-mode variational structure to ensure system power balance.

### 3.2 ADMM distributed power optimization process

Traditional centralized optimization accepts all state information. It makes the optimal control decision of the system, while distributed ADMM performs local optimization for each subsystem and achieves global optimization through iterative optimization among subsystems.

Define  $P_{W,ref}$ ,  $P_{S,ref}(k)$ , and  $P_{b,ref}(k)$  as the power reference values solved by ADMM. As shown in Figure 3, the ADMM distributed computing framework is established: S1 represents the wind power generation subsystems, S2 represents the photovoltaic power generation subsystems, and S3 represents the battery subsystems. First, the ADMM solves for the power reference values  $P_{W,ref}$ ,  $P_{S,ref}(k)$ , and  $P_{b,ref}(k)$  of the wind, PV, and battery subsystems, respectively. Second, the iterative update of the Gaussian penalty function  $\rho$  is added to ensure the stability and speed of the algorithm optimization.

The steps for solving for ADMM- $\rho$  are as follows:

**Step 1:** S1 starts solving the  $P_{W,ref}$  of the power reference value of the wind power generation subsystems.

**Step 2:** S1 passes the calculated value of  $P_{W,ref}$  to S2 through the contact line.

**Step 3:** S2 solves the power reference value of the photovoltaic power generation subsystems  $P_{S,ref}(k)$ .

**Step 4:** S2 passes the value of the calculation result  $P_{S,ref}(k)$  to S3 through the contact line.

**Step 5:** S3 solves the predicted value of the power reference for the battery subsystems  $P_{b,ref}(k)$ .

**Step 6:** S3 passes the value of the calculation result  $P_{b,ref}(k)$  to S1 through the contact line.

**Step 7:** Solves  $\lambda$  by taking the value  $\rho$  for  $P_{W,ref}$ ,  $P_{S,ref}(k)$ ,  $P_{b,ref}(k)$ , and  $k-1$  iterations.

**Step 8:** Update the value of  $\rho$ .

### 3.3 ADMM optimization objective function and constraints

The quadratic objective function for the wind power generation subsystems is represented as follows:

$$\min f_1(P_{W,ref}) = \frac{1}{2} h_1 P_{W,ref}^2, \quad (14)$$

where  $h_1$  is a constant to where  $h_1$  is a positive constant, and its larger values lead to faster convergence but may result in decreased stability. The constraints of the wind power generation subsystems are as follows:

$$\begin{cases} P_T(k) + P_{b,ref}(k) - P_{W,ref}(k) - P_{S,ref}(k) = 0, \\ 0 \leq P_{W,ref}(k) \leq P_{W,max}, \\ 0 \leq d_b(k) \leq d_{b,max}, \\ |i_b(k)| \leq i_{b,max}. \end{cases} \quad (15)$$

The objective function of the photovoltaic power generation subsystems is as follows:

$$\min f_2(P_{S,ref}) = \frac{1}{2} h_2 P_{S,ref}^2, \quad (16)$$

where  $h_2$  is a constant to where  $h_2$  is a positive constant, and its larger values lead to faster convergence but may result in decreased stability.

The constraints of the photovoltaic power generation subsystems are as follows:

$$\begin{cases} P_T(k) + P_{b,ref}(k) - P_{W,ref}(k) - P_{S,ref}(k) = 0, \\ 0 \leq P_{S,ref}(k) \leq P, \\ 0 \leq d_b(k) \leq d_{b,max}, \\ |i_b(k)| \leq i_{b,max}. \end{cases} \quad (17)$$

The objective function of the battery subsystems is expressed as follows:

$$\min f_3(P_{b,ref}) = \frac{1}{2} h_3 P_{b,ref}^2, \quad (18)$$

where  $h_3$  is a constant to where  $h_3$  is a positive constant, and its larger values lead to faster convergence but may result in decreased stability.

The constraints for the battery subsystems are as follows:

$$\begin{cases} P_T(k) + P_{b,ref}(k) - P_{W,ref}(k) - P_{S,ref}(k) = 0, \\ |P_{b,ref}(k)| \leq P_{b,max}, \\ 0 \leq d_b(k) \leq d_{b,max}, \\ |i_b(k)| \leq i_{b,max}. \end{cases} \quad (19)$$

$x$  indicates that the optimization objective vector is represented as follows:

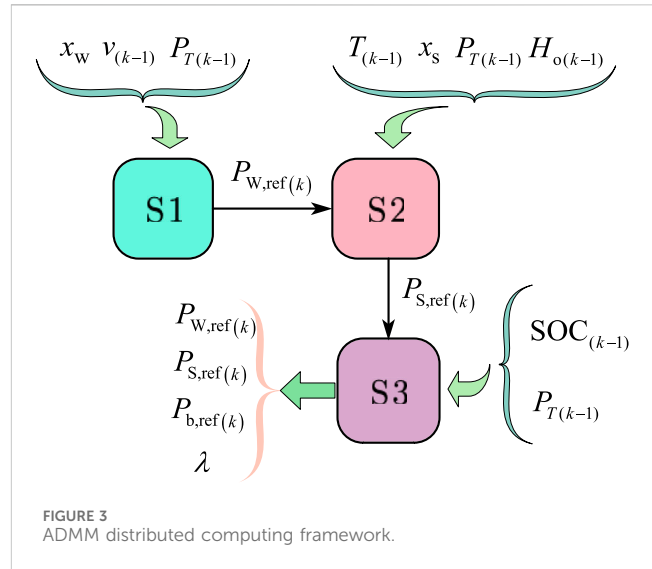
$$x = \begin{bmatrix} x_1 \\ x_2 \\ x_3 \end{bmatrix} = \begin{bmatrix} P_{W,ref} \\ P_{S,ref} \\ P_{b,ref} \end{bmatrix}. \quad (20)$$

According to (14), (16), and (18), the whole system's optimization objective function is as follows:

$$\min f(x) = \frac{1}{2} x^T H x, \quad (21)$$

$$H = \begin{pmatrix} h_1 & 0 & 0 \\ 0 & h_2 & 0 \\ 0 & 0 & h_3 \end{pmatrix}, \quad (22)$$

where  $H$  is the coefficient matrix of the global optimization objective function of the system, which is a semi-positive definite symmetric matrix if the value of the diagonal element is immense. The corresponding wind power reference value, photovoltaic power reference value, or battery power reference value will have a more significant impact on the objective function.



### 3.4 Distributed ADMM- $\rho$ iterative design

The ADMM- $\rho$  is used to solve the power references  $P_{W,ref}$ ,  $P_{S,ref}(k)$ ,  $P_{b,ref}(k)$ , and  $\lambda$  for each subsystem. The constraints in the standalone hybrid generation systems are rewritten in the form of sets, and the convex sets are defined as follows:

$$C_1 = \{P_{W,ref}(k), P_{S,ref}(k), P_{b,ref}(k) \mid P_T(k) + P_{b,ref}(k) - P_{W,ref}(k) - P_{S,ref}(k) = 0\}, \quad (23)$$

$$C_2 = \{P_{W,ref}(k) \mid 0 \leq P_{W,ref}(k) \leq P_{W,max}\}, \quad (24)$$

$$C_3 = \{P_{S,ref}(k) \mid 0 \leq P_{S,ref}(k) \leq P_{S,max}\}, \quad (25)$$

$$C_4 = \{P_{b,ref}(k) \mid |P_{b,ref}(k)| \leq P_{b,max}\}, \quad (26)$$

$$C_5 = \{d_b(k) \mid 0 \leq d_b(k) \leq d_{b,max}\}, \quad (27)$$

$$C_6 = \{i_b(k) \mid |i_b(k)| \leq i_{b,max}\}. \quad (28)$$

Define the auxiliary variable  $z$  and the indicator function  $g(z)$  such that  $z = x$ .

$$\begin{cases} \min(f(x) + g(z)) \\ s.t. x = z \\ \text{dorm } f = C_1 \cap C_2 \cap C_3 \cap C_4 \cap C_5 \cap C_6, \end{cases} \quad (29)$$

where  $\text{dorm } f$  is the domain of definition of the function  $f$  and  $g$  is the indicator function on  $C_2 \cap C_3 \cap C_4 \cap C_5 \cap C_6$ .

$$g(z) = \begin{cases} 0, z \in C_2 \cap C_3 \cap C_4 \cap C_5 \cap C_6 \\ +\infty, z \notin C_2 \cap C_3 \cap C_4 \cap C_5 \cap C_6 \end{cases} \quad (30)$$

The augmented Lagrangian function for constructing each suboptimization problem is as follows:

$$L_\rho(x, z, \lambda) = f(x) + g(z) + \lambda^T \|x - z\|_2^2 + \frac{\rho}{2} \|x - x_{ref} + \xi \cdot E\|_2^2, \quad (31)$$

where  $\lambda$  is the Lagrangian multiplier,  $\rho$  is the Gaussian penalty function,  $x_{ref}$  is the reference value of the vector  $x$ , and  $\xi$  is the error factor between  $x_{ref}$  and  $x$ ,  $\xi > 0$ .

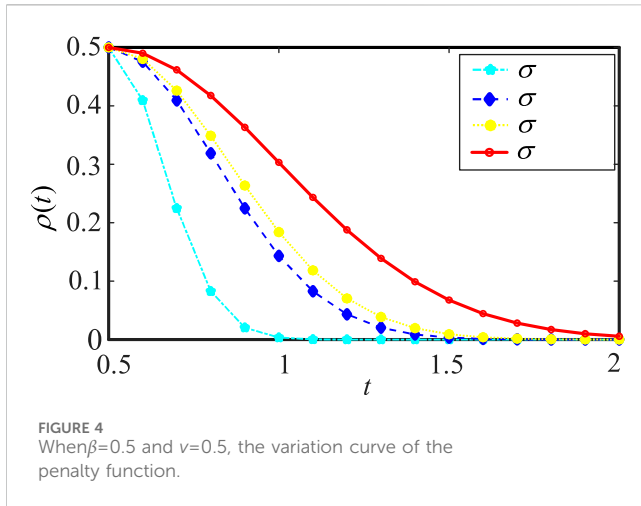


FIGURE 4 When  $\beta=0.5$  and  $\nu=0.5$ , the variation curve of the penalty function.

The iterative calculation order is  $x_1 \rightarrow z_1 \rightarrow \lambda_1 \rightarrow \rho_1 \rightarrow x_2 \rightarrow z_2 \rightarrow \lambda_2 \rightarrow \rho_2 \rightarrow x_3 \rightarrow z_3 \rightarrow \lambda_3 \rightarrow \rho_3$ . Using ADMM, the iterative solution steps repeat the following steps for  $i=1,2,3 \dots$  and  $k=1, 2, 3 \dots$ :

$$x_i^k = \arg \min_{x_i} (f(x_i) + \lambda_i^{k-1} \|x_i - z_i^{k-1}\|_2^2), \quad (32)$$

$$z_i^k = \arg \min_{z_i} \left( g(z_i) + \lambda_i^{k-1} \|x_i^k - z_i\|_2^2 + \frac{\rho_i^{k-1}}{2} \|x_i - x_{i,ref} + \xi\|_2^2 \right), \quad (33)$$

$$\lambda_i^k = \lambda_i^{k-1} + \rho_i^{k-1} (x_i^k - z_i^k), \quad (34)$$

$$\rho_i^k (\rho_i^{k-1}) = \beta \exp \left[ -\frac{(\rho_i^{k-1} - \nu)^2}{\sigma} \right], \quad (35)$$

where the penalty coefficient  $\beta$ , neighborhood size factor  $\sigma$ , and the neighborhood center  $\nu$  are all greater than zero, and the value of the parameter  $\nu$  determines the location of the penalized region.

When  $t \in [\nu, +\infty)$ , the Gaussian penalty function  $\rho(t)$  takes a large value at the initial trial stage and decreases rapidly, but at the later stages of the iteration,  $\rho(t)$  is basically unchanged and exhibits some localization.

The size of the penalty region is characterized by the parameter  $\sigma$ , which gives different results for different values of  $\sigma$ .

When  $\beta = 0.5$  and  $\nu = 0.5$ , the penalty function  $\rho(t)$  will change over time with the difference in the value of  $\sigma$  (Figure 4).

The change of the penalty function  $\rho(t)$  is roughly in line with the normal distribution. When the value of  $\sigma$  is more significant than 0.25, then  $\rho(t)$  changes relatively gently throughout the iteration process. When the value of  $\sigma$  is less than 0.25, it decreases rapidly throughout the iteration process. In this paper, we specify  $\sigma = 0.25$ .

Convergence criteria:

$$\|r^{(k)}\|_2^2 = \|x_i^k - z_i^k\|_2^2 \leq \epsilon_{pri}, \quad (36)$$

$$\|s^{(k)}\|_2^2 = \|\rho_i(z_i^k - z_i^{k-1})\|_2^2 \leq \epsilon_{dul}, \quad (37)$$

where  $r^{(k)}$  and  $s^{(k)}$  are the primal and dual residual after the  $k$  times iteration, corresponding to the upper residual tolerance limits of  $\epsilon_{pri}$  and  $\epsilon_{dul}$ .

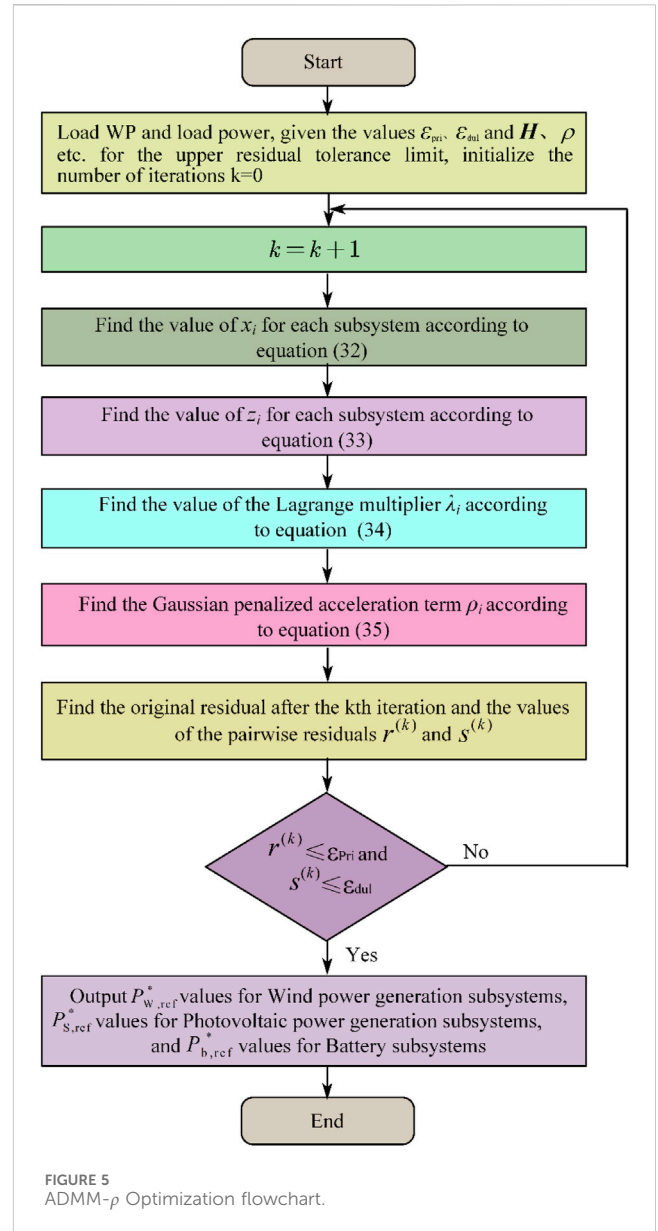


FIGURE 5 ADMM- $\rho$  Optimization flowchart.

The flowchart of ADMM algorithm optimization is shown in Figure 5.

The specific process of ADMM- $\rho$  iterative optimization is as follows.

- (1) Load the WP data, SOC data, and load power; initialize parameters such as  $H, \xi, \epsilon_{pri}$ , and  $\epsilon_{dul}$ ; and make the number of iterations  $k = 0$ ;
- (2)  $k=k+1$ ;
- (3) Wind power generation subsystems are subjected to the  $k$ -times iteration, solving  $x_1$  according to Eq. 32,  $z_1$  according to Eq. 33,  $\lambda_1$  according to Eq. 34, and  $\rho_1$  according to Eq. 35.
- (4) Wind power generation subsystems pass the calculation results  $P_{W,ref}^{(k)}$  to the photovoltaic power generation subsystems through the contact line.

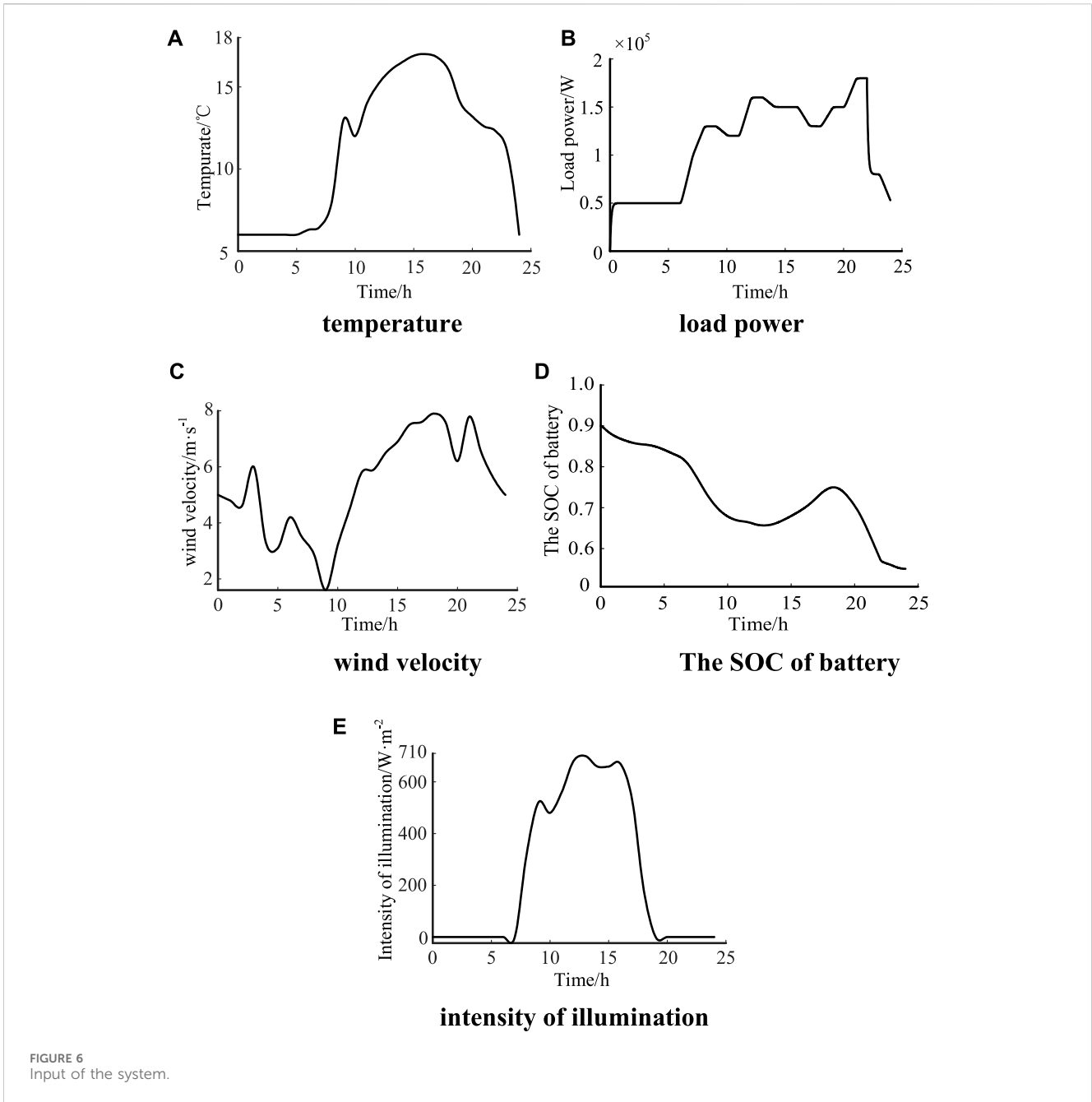
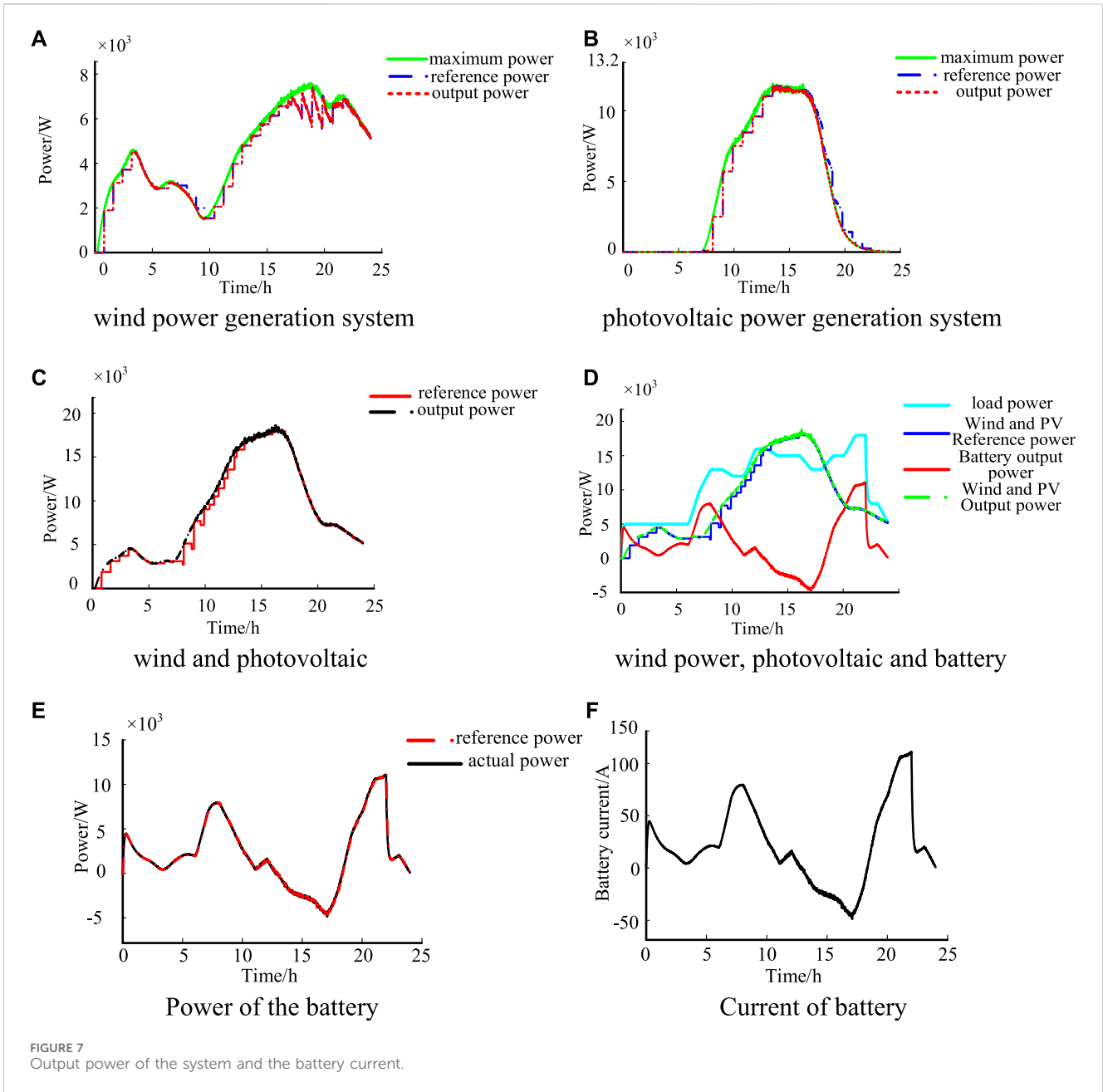


FIGURE 6 Input of the system.

- (5) Photovoltaic power generation subsystems are subjected to the  $k$  times iteration, solving  $x_2$  according to Eq. 32,  $z_2$  according to Eq. 33,  $\lambda_2$  according to Eq. 34, and  $\rho_2$  according to Eq. 35.
- (6) The photovoltaic power generation subsystems transfer the calculation results  $P_{S,ref}^{(k)}$  of the battery subsystems through the contact line.
- (7) Battery subsystems are subjected to the  $k$  times iteration, solving  $x_3$  according to Eq. 32,  $z_3$  according to Eq. 33,  $\lambda_3$  according to Eq. 34, and  $\rho_3$  according to Eq. 35.
- (8) The battery subsystems pass the  $k$  sub-corrected value to the photovoltaic power generation subsystems through the contact line.
- (9) The photovoltaic power generation subsystems pass the  $k$  sub-corrected values to the wind power generation subsystems through the contact line.
- (10) The photovoltaic power generation subsystems pass the  $k$  sub-corrected values to the wind power generation subsystems through the contact line.
- (11) Calculate the values of residuals  $r^{(k)}$  and  $s^{(k)}$  according to Eqs 36, 37.
- (12) Compare whether  $r^{(k)} \leq \epsilon_{pri}$  and  $s^{(k)} \leq \epsilon_{dul}$  hold simultaneously. If they hold, stop the iteration and output the calculation results to obtain the optimal solutions  $P_{W,ref}^*$ ,  $P_{S,ref}^*$  and  $P_{b,ref}^*$  for the three subsystem powers; otherwise,  $k=k+1$ , go back to step (2), and





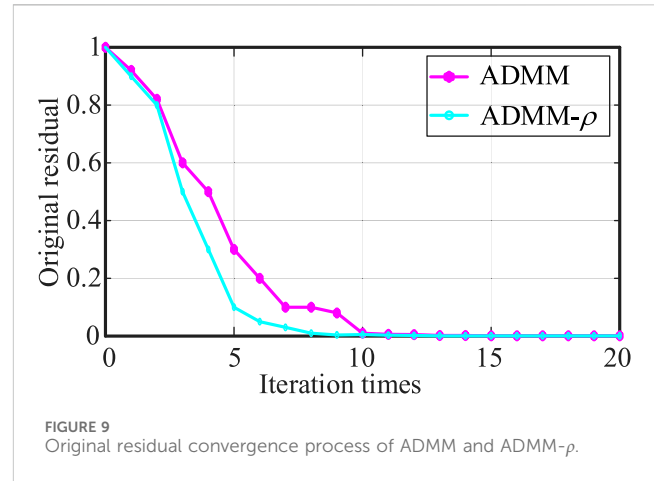
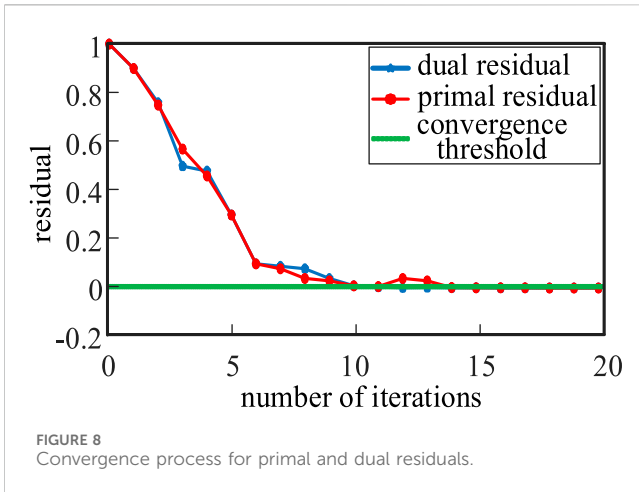
repeat the above steps until the residual convergence is satisfied.

## 4 Simulation verification and result analysis

### 4.1 Experimental data

In this paper, the WP data and load power for a day in a region in southern China are selected as the inputs to the system (Figure 6): As shown in Figure 6A, the temperature range is 6°C–17°C. As shown in Figure 6E, the range of light intensity is 0.002–700 W/m<sup>2</sup>. As shown in Figure 6C, the range of wind

speed is 1.6–7.9 m/s. As shown in Figure 6D, the range of SOC is 0.4–0.9. As shown in Figure 6B, and the range of load power is 5–18 kW. The provided data include temperature, load power, wind speed, and battery SOC, with consistent sharp, smooth, stable constant changes. However, the amplitude of each parameter is relatively limited. According to Y. Wang et al. (2017b), the convergence of the ADMM algorithm depends mainly on the concavity and convexity of the variables. In this paper, Eqs 23–28 define its convex set form, and the magnitude of each parameter does not affect its concavity and convexity. These data can be used as input to and are representative of the distributed ADMM power optimal control for standalone hybrid generation systems. Taking  $\xi = 0.001$  and  $\varepsilon_{pri} = \varepsilon_{dul} = 0.001$ , make  $h_1 = 25$ ,  $h_2 = 32$ , and  $h_3 = 15$ . Let the



maximum value of the reference power of PV in the constraints be 11.9kW, the maximum value of the reference power of wind be 7.6kW, and the capacity of the battery be 1000Ah.

## 4.2 Simulation results

The standalone wind and storage hybrid power generation system is simulated, and 24 h are selected as the simulation time. The power of the wind and photovoltaic power generation subsystems and the power and current of the battery subsystems are shown in Figure 7.

Take 21:00–22:00 in 24 h as an example. The load power is a constant value of 18kW, the reference power range of the wind power generation subsystems obtained by the ADMM solution is 6716.0–6697.0 W, the reference power range of the photovoltaic power generation subsystems is 262.6–654.9 W, and the total output reference power range of the wind and photovoltaic power generation subsystems is 6978.6–7351.9 W. However, the total output actual power range of the wind and photovoltaic power generation subsystems is 7303.0–6987.0 W, the wind and photovoltaic subsystems cannot satisfy the power demand of the load, the battery subsystems have an output power of 10,697.0–11013.0 W, and the controller adjusts the duty cycle of the converter so that the battery subsystems are all working in maximum power tracking from 21:00–22:00 mode so that the battery is in a discharged state. The whole system is in an insufficient state over 21:00–22:00. According to the simulation results, during 0–24 h, the system is in a sufficient state in the phase 12:00–18:00, in a balanced state in the phase 12:00–18:00, and in a deficient state in the phases 0:00–12:00 and 18:00–24:00. During 12:00–18:00, the wind power and photovoltaic power generation subsystems are working in the load tracking mode in which the battery absorbs excess power. For 0:00–12:00 and 18:00–24:00, the wind and photovoltaic power generation subsystems are operating in maximum power tracking mode, and the battery subsystems make up the difference in power to stabilize the system.

Figure 7E shows the power curve of the battery; the positive power indicates that the battery is discharging, and the negative power indicates that the battery is charging. Due to the rapid

response of the battery, its actual power value curve coincides with the power reference value curve, which ensures the stable operation of the system. Figure 7A shows the maximum, reference and output power of wind power systems; Figure 7B shows the maximum, reference and output power of the PV systems; Figure 7C shows the reference power and output power of wind and PV; Figure 7D shows the actual output power of wind, PV and battery, load power.

Figure 7F shows the current waveform of the battery; the current is positive battery discharging, and the current is negative battery charging. At 0:00–12:00 and 18:00–24:00, the battery is discharging, and at 12:00–18:00, the battery is charging.

## 4.3 Convergence analysis of the ADMM algorithm

To ensure that the output power of the hybrid power generation system satisfies the user's load power demand, the ADMM algorithm must calculate the reference value of the output power of the local controller of the wind, light, and battery subsystems in real-time based on variations in the load and different weather conditions during the simulation process. This calculation alters the duty cycle of the DC/DC converter and adjusts the output power of the wind, light, and battery subsystems. As a result, multiple computations must be conducted to address the issue during the 24-h simulation. Due to space constraints, only the changes in values of the original residuals, pairwise residuals, and convergence thresholds with the number of iterations for a particular calculation are presented. The convergence process of original and pairwise residuals is displayed in Figure 8. As observed, the pairwise residuals attained convergence threshold requirements in the 10th iteration, while the original residuals reached the same in the 14th iteration. The ADMM algorithm exhibits superior capability in finding optimal solutions and achieving convergence speed when addressing the power optimization challenges in standalone hybrid generation systems.

For ADMM and ADMM- $\rho$  with the addition of a Gaussian penalty function, the convergence process of their original residuals is shown in Figure 9. It can be seen that ADMM- $\rho$  reaches

convergence the 14th time. This can be compared with ADMM, which is also a distributed optimization, which reaches convergence the 16th time, with ADMM- $\rho$ , which makes the residuals converge to the convergence threshold of 0.001 in a shorter time, and with ADMM- $\rho$ , which has a better convergence characteristic. This improves the optimization ability and convergence speed of the standalone hybrid generation systems for wind, solar, storage, and electricity generation.

## 5 Conclusion

For the power optimization problem of standalone hybrid generation systems with wind and storage, an ADMM- $\rho$  distributed optimization method based on the Gaussian penalty function is proposed, and the ADMM algorithm is used in the solution of this optimization problem. The ADMM algorithm can make full use of the decomposability of the system to solve the multivariate optimization alternately, with good optimization-seeking ability; at the same time, solving the power optimization problem of the standalone hybrid generation systems of wind power and storage is not subject to the limitation of the system size. Finally, the comparison shows that ADMM- $\rho$  with a Gaussian penalty function can converge the residuals to the threshold range more quickly and with better convergence properties than the ADMM method. Power optimal control of standalone hybrid generation systems is a complex and challenging problem. The distributed ADMM approach provides an effective optimization method but still requires further research and improvement to solve various problems in practical applications. Such research can explore aspects such as more efficient information exchange mechanisms, optimization models that consider uncertainty and economics, and integration with energy markets to further improve the performance of optimal power control for standalone hybrid generation systems.

## References

- Bottou, L., Curtis, F. E., and Nocedal, J. (2018). Optimization methods for large-scale machine learning. *SIAM Rev.* 60 (2), 223–311. doi:10.1137/16M1080173
- Chang, X., Liu, S., Zhao, P., and Song, D. (2019). A generalization of linearized alternating direction method of multipliers for solving two-block separable convex programming. *J. Comput. Appl. Math.* 357, 251–272. doi:10.1016/j.cam.2019.02.028
- Feroldi, D., Rullo, P., and Zumoffen, D. (2015). Energy management strategy based on receding horizon for a power hybrid system. *Renew. Energy* 75, 550–559. doi:10.1016/j.renene.2014.09.056
- Feroldi, D., and Zumoffen, D. (2014). Sizing methodology for hybrid systems based on multiple renewable power sources integrated to the energy management strategy. *Int. J. Hydrogen Energy* 39 (16), 8609–8620. doi:10.1016/j.ijhydene.2014.01.003
- Kang, L., Wang, J., Liu, J., and Ye, D. (2018). Survey on parallel and distributed optimization algorithms for scalable machine learning. *J. Softw.* 29 (1), 109–130. doi:10.13328/j.cnki.jos.005376
- Le, J., Liao, X., Zhang, Y.-T., Chang, J.-X., and Lu, J. (2020). Review and prospect on distributed model predictive control method for power system. *Automation Electr. Power Syst.* 44 (23), 179–191. doi:10.7500/AEPS20200212005
- Parikh, N. (2014). Proximal algorithms. *Found. Trends<sup>®</sup> Optim.* 1 (3), 127–239. doi:10.1561/2400000003
- Suo, X., Zhao, S., Ma, Y., and Dong, L. (2021). New energy wide area complementary planning method for multi-energy power system. *IEEE Access* 9, 157295–157305. doi:10.1109/ACCESS.2021.3130577
- Tan, K. M., Babu, T. S., Ramachandaramurthy, V. K., Kasinathan, P., Solanki, S. G., and Raveendran, S. K. (2021). Empowering smart grid: a comprehensive review of energy storage technology and application with renewable energy integration. *J. Energy Storage* 39, 102591. doi:10.1016/j.est.2021.102591
- Wang, X., Wang, Z., Zhang, X., Bao, G., and Gong, W. (2017a). Distributed predictive control of stand-alone hybrid generation systems. *Acta Energetica Solaris Sin.* 38 (9), 2403–2411. doi:10.19912/j.0254-0096.2017.09.011
- Wang, Y., Wang, S., and Wu, L. (2017b). Distributed optimization approaches for emerging power systems operation: a review. *Electr. Power Syst. Res.* 144, 127–135. doi:10.1016/j.epr.2016.11.025
- Wright, S. J. (2015). Coordinate descent algorithms. *Math. Program.* 151 (1), 3–34. doi:10.1007/s10107-015-0892-3
- Xin, Y., Chen, W., Sun, R., Shi, Y., Liu, C., Xia, Y., et al. (2019). Analytical switching loss model for GaN-based control switch and synchronous rectifier in low-voltage buck converters. *IEEE J. Emerg. Sel. Top. Power Electron.* 7 (3), 1485–1495. doi:10.1109/JESTPE.2019.2922389
- Zhao, J., and Yuan, X. (2016). Multi-objective optimization of stand-alone hybrid PV-wind-diesel-battery system using improved fruit fly optimization algorithm. *Soft Comput.* 20 (7), 2841–2853. doi:10.1007/s00500-015-1685-6

## Data availability statement

The original contributions presented in the study are included in the article/Supplementary material; further inquiries can be directed to the corresponding author.

## Author contributions

TW: conceptualization, methodology, writing—original draft. YW: validation, writing—review and editing. JY: validation, writing—review and editing.

## Funding

The author(s) declare that no financial support was received for the research, authorship, and/or publication of this article.

## Conflict of interest

The authors declare that the research was conducted in the absence of any commercial or financial relationships that could be construed as a potential conflict of interest.

## Publisher's note

All claims expressed in this article are solely those of the authors and do not necessarily represent those of their affiliated organizations or those of the publisher, the editors, and the reviewers. Any product that may be evaluated in this article, or claim that may be made by its manufacturer, is not guaranteed or endorsed by the publisher.